



# CHORUS

This is the accepted manuscript made available via CHORUS. The article has been published as:

## Direct Observations of a Dynamically Driven Phase Transition with in situ X-Ray Diffraction in a Simple Ionic Crystal

Patricia Kalita, Paul Specht, Seth Root, Nicholas Sinclair, Adam Schuman, Melanie White, Andrew L. Cornelius, Jesse Smith, and Stanislav Sinogeikin

Phys. Rev. Lett. **119**, 255701 — Published 21 December 2017

DOI: [10.1103/PhysRevLett.119.255701](https://doi.org/10.1103/PhysRevLett.119.255701)

# Direct Observations of a Dynamically-Driven Phase Transition with *In-situ* X-ray Diffraction in a Simple Ionic Crystal

Pat Kalita,\* Paul Specht, and Seth Root  
*Sandia National Laboratories, Albuquerque, NM 87125*

Nicholas Sinclair and Adam Schuman  
*Dynamic Compression Sector, Institute for Shock Physics,  
Washington State University, Argonne, IL 60439*

Melanie White and Andrew L. Cornelius  
*High Pressure Science and Engineering Center, University of Nevada Las Vegas, Las Vegas NV 89154*

Jesse Smith and Stanislav Sinogeikin  
*High-Pressure Collaborative Access Team, Carnegie Institution of Washington, Argonne, IL 60439*

We report real-time observations of a phase transition in the ionic solid  $\text{CaF}_2$ , a model  $\text{AB}_2$  structure in high pressure physics. Synchrotron x-ray diffraction coupled with dynamic loading to 27.7 GPa, and separately with static compression, follows, *in situ*, the fluorite to cotunnite structural phase transition, both on nanosecond and on minute time scales. Using Rietveld refinement techniques, we examine the kinetics and hysteresis of the transition. Our results give insight into the kinetic timescale of the fluorite-cotunnite phase transition under shock compression, which is relevant to a number of isomorphic compounds.

Understanding the behavior of compression-driven phase transformations, their pathways, and kinetics, lies at the core of contemporary static and dynamic compression research at advanced light sources [1]. Traditionally, shock compression research infers phase transitions from continuum level measurements and uses corresponding static compression experiments, shock-recovery studies, or calculations to deduce the resulting phase. The advent of synchrotron facilities where shock compression is coupled with real time x-ray diffraction (XRD) now allows for microstructural identification of phase transitions and monitoring of transition kinetics [2–4]. Prior dynamic diffraction experimental work has focused on melting, crystallization, and the solid-solid phase transition in a simple monotonic solid. Here, we present direct observation of the complex solid-solid phase transition in an  $\text{AB}_2$  ionic crystal:  $\text{CaF}_2$ .

Somewhat surprisingly, given the relative simplicity of  $\text{CaF}_2$  and the many high-pressure studies[5–11], little data is available from dynamic compression. Upon static compression to 9 GPa (hydrostatic) or 11-16 GPa (non-hydrostatic),  $\text{CaF}_2$  undergoes a phase transition from the cubic fluorite structure ( $Fm\bar{3}m$ ,  $Z=4$ ) to an orthorhombic cotunnite-type structure ( $Pnam$ ,  $Z=4$ ) [7, 12, 13]. The sensitivity to non-hydrostatic conditions on static compression suggests a sensitivity to dynamic compression.

Early shock compression experiments reported observing the cotunnite phase of  $\text{CaF}_2$  using x-ray diffraction on recovered samples [14, 15]. More recently, researchers made real-time measurements on  $\text{CaF}_2$  using continuum-scale velocimetry measurements that suggested the presence of a phase transition under shock [16, 17]. However, these measurements do not provide time-resolved lattice

or structure information. The transition observed in the velocimetry data was assumed to be fluorite to cotunnite analogous to static compression studies.

In this Letter, we report the method and results from the first direct, real-time, microstructural, atomic-scale observations of a shock-driven phase transition in  $\text{CaF}_2$ . Synchrotron XRD experiments are coupled with plate impact launchers and Photonic Doppler Velocimetry (PDV) to follow, *in-situ*, the solid-solid phase transition in shock-compressed  $\text{CaF}_2$ . The results are compared with our XRD studies under static compression and high temperatures, designed to mimic the states achieved in shock compression. We discuss the kinetics and the reversibility of the transition both qualitatively and quantitatively. Finally we present Hugoniot equation of state data for 75% dense porous  $\text{CaF}_2$ .

Plate-impact shock wave experiments coupled with dynamic XRD were performed on  $\text{CaF}_2$  powder compacts. Lexan<sup>®</sup> flyer plates were accelerated from 2 to 6 km/s using a 2-stage light gas gun or powder gun that impacted finely ground  $\text{CaF}_2$  powders  $\sim 75\pm 1\%$  theoretical maximum density (TMD, single crystal  $\rho_0 = 3.18 \text{ g/cm}^3$ ). The back surface of each sample was mounted to a TPX<sup>®</sup> window [18, 19]. Experiments were performed at the Dynamic Compression Sector (DCS) at the Advanced Photon Source (APS). A focused pink x-ray beam is used for single-pulse XRD images ( $\sim 100 \text{ ps}$  duration). A four-image XRD detector allows the study of temporal evolution of structure during shock compression by recording four XRD snapshots [20].

Figure 1 inset shows a schematic view of the experimental configuration. The Lexan projectile impacts  $\text{CaF}_2$ , sending a shock wave through the sample. A 4-

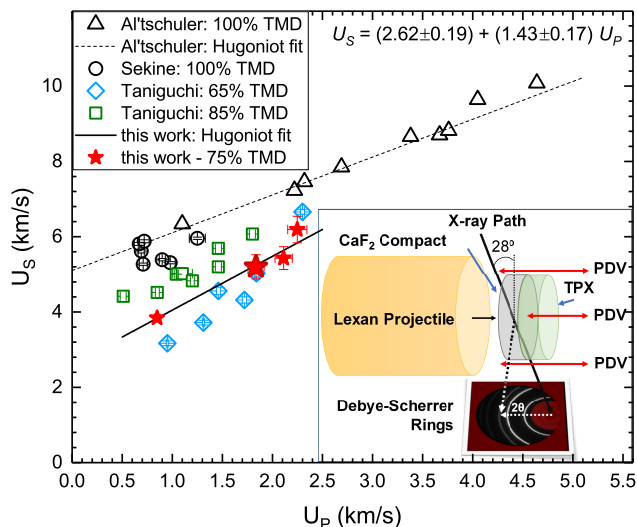


FIG. 1. Experimental Hugoniot data in the shock velocity ( $U_S$ ) vs. particle velocity ( $U_P$ ) plane, for five shots (two data points are overlapped). Five solid red stars (two are overlapped) represent  $\text{CaF}_2$  at  $75 \pm 1\%$  TMD investigated in this work. Open symbols refer to literature data for  $\text{CaF}_2$  at various initial densities [17, 21, 22].

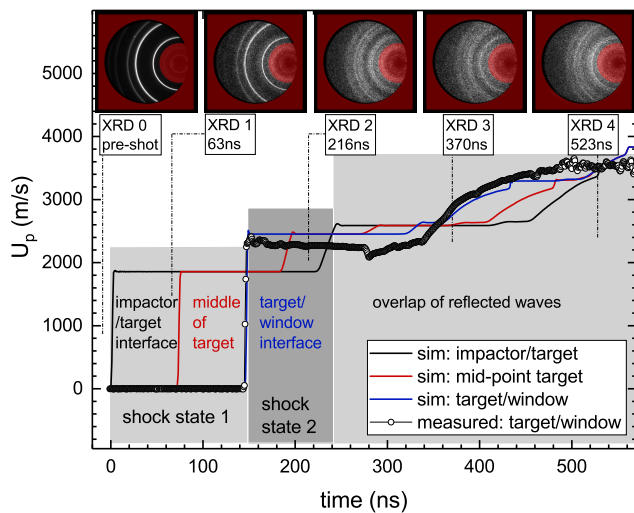


FIG. 2. Example of the temporal connection between XRD images acquired and the evolution of the shock event as measured by PDV (circles). Dashed lines show times when Debye-Scherrer rings were recorded (corresponding diffraction shown in Fig. 3). Simulated  $U_P$  traces (solid lines, using the Hugoniot of reference [21]) illustrate the shock state of the sample at three locations.

78 channel PDV system [23] records the impact time and  
 79 the particle velocity ( $U_P$ ) at the  $\text{CaF}_2$ /TPX interface.  
 80 The first abrupt change in the interface  $U_P$  indicates  
 81 the initial shock arrival time at the  $\text{CaF}_2$ /TPX inter-  
 82 face (Fig. 2). The shock velocity is calculated from  
 83 the known thickness and shock wave transit time. Us-  
 84 ing the Lexan Hugoniot [18] along with the measured

85 impact velocity, we apply the Rankine-Hugoniot jump  
 86 conditions [24] and the *Monte Carlo* impedance match-  
 87 ing [20, 25] method, to determine the  $\text{CaF}_2$  density ( $\rho$ ),  
 88 stress ( $\sigma$ ), and  $U_P$ . The resulting Hugoniot states are  
 89 plotted in  $U_S$ - $U_P$  space in Fig. 1. A linear fit to our data  
 90 yields  $U_S = (2.62 \pm 0.19) + (1.43 \pm 0.17)U_P$  with a covari-  
 91 ance of  $-0.030994$  between the parameters. Comparison  
 92 with Ref. 22 shows our Hugoniot data is consistent with  
 93 their 65% and 85% dense  $\text{CaF}_2$  data. Experimental de-  
 94 tails, a list of shots and Hugoniot data are in [20].

### 95 XRD and Analysis of the Shock Event

96 Fig. 3 (a and b) show dynamic XRD data, measured  
 97 as a function of time, and hence shock state. Details  
 98 of the experiments are in [20]. Static compression data  
 99 (Fig. 3(c)) will be addressed later. Starting at  $t=0$ , a  
 100 planar shock wave traverses the sample and produces the  
 101 maximum stress state (“state 1” later used in the stress-  
 102 unit cell volume analysis). When the shock reaches the  
 103 lower impedance TPX, a release wave is generated trav-  
 104 eling back into the  $\text{CaF}_2$  lowering the stress. When the  
 105 initial shock reaches the TPX free surface, a release fan  
 106 travels back through the window. Later the sample ex-  
 107 periences multiple wave interactions, generating complex  
 108 stress gradients and obscuring the stress state (Fig. 2 and  
 109 Fig. S7 in [20]).

110 Depending on the shock stress  $\text{CaF}_2$  responds in dif-  
 111 ferent fashion. Figure 3(a) shows the dynamic XRD  
 112 data for  $\text{CaF}_2$  shock-compressed to a maximum stress  
 113 of 7.8 GPa. At 105 ns after impact, the shock wave has  
 114 traveled through 30% of the sample. The cubic lattice  
 115 is compressed, as indicated by the diffraction lines mov-  
 116 ing towards lower  $d$ -spacings, meaning increased density.  
 117 The shifted diffraction lines appear as shoulders on the  
 118 right of ambient lines, because the x-ray beam is passing  
 119 through both shocked and unshocked regions in  $\text{CaF}_2$ .  
 120 By 259 ns the shock wave has made it through 90% of  
 121 the sample, with only 10% still at ambient pressure. At  
 122 412 ns and 566 ns, as the stress continues to decrease,  
 123 because of release waves, the diffraction lines move back  
 124 towards higher  $d$ -spacings, meaning lower density. Hence  
 125 the evolution of density (diffraction lines) mirrors the  
 126 shock event unfolding in the sample. Line broadening  
 127 is attributed to measurement over multiple stress states.

### 128 Shock-Driven Phase Transition

129 Figure 3(b) shows the unfolding of the  $\text{CaF}_2$  fluorite  
 130 to cotunnite phase transition under shock compression  
 131 to 22.6 GPa. The sample starts in its fluorite structure  
 132 (XRD-0). The phase transition to cotunnite initially ap-  
 133 pears in coexistence with the fluorite phase, as the shock  
 134 wave creates a stress state of 22.6 GPa, while in front of  
 135 the wave  $\sim 60\%$  of the sample is still at 0 GPa (XRD-  
 136 1). Next, the cotunnite phase becomes more prevalent  
 137 (XRD-2, 216ns)  $\sim 25\%$  of the sample being between 10.5  
 138 and 22.6 GPa, while  $\sim 75\%$  of the sample is at 10.5 GPa,  
 139 because of the impedance mismatch between the  $\text{CaF}_2$   
 140 and TPX window[20]. At this time, both fluorite and co-

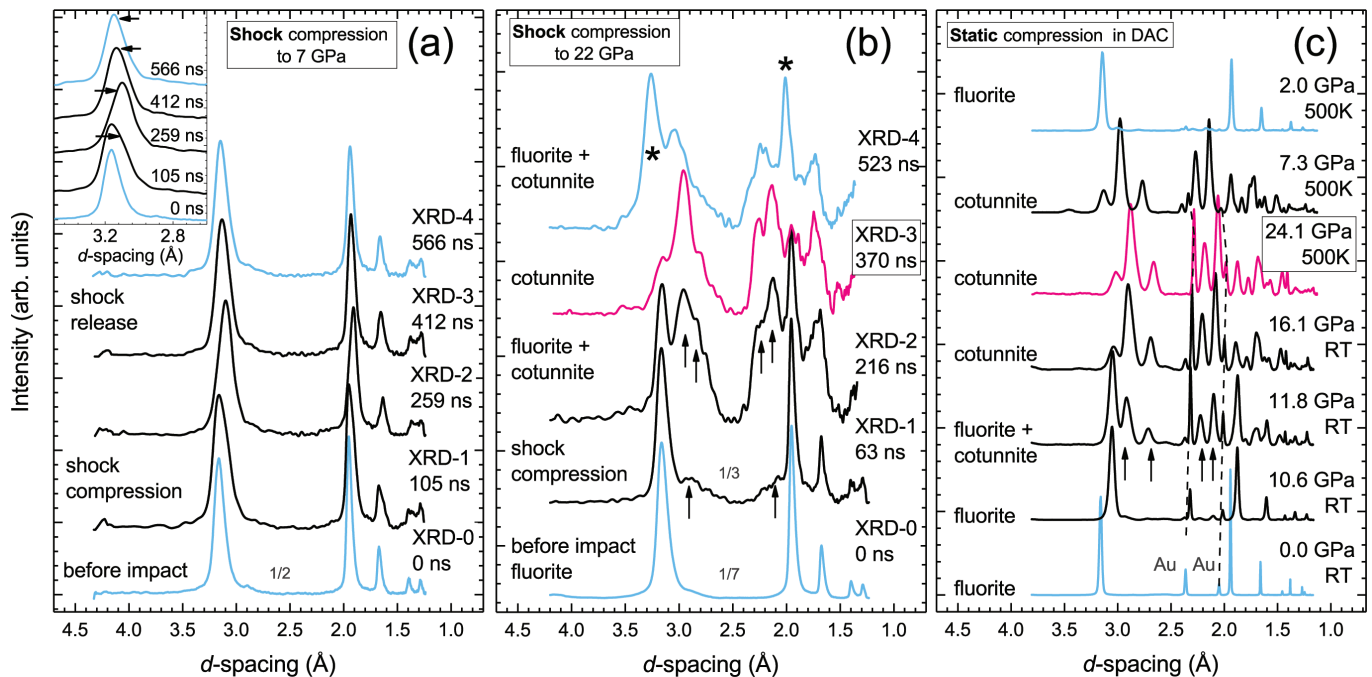


FIG. 3. *In-situ* XRD patterns under shock-compression measured as a function of time, showing (a) a shot to 7.8 GPa, below the phase transition conditions, (b) a shot to 22.6 GPa, with a phase transition and (c) *in-situ* XRD patterns under static compression in DAC as a function of pressure and temperature. Times are relative to impact ( $t=0$ ). Inset in (a) shows a zoom of the [111] diffraction line, where shock compression and release are seen in the evolution of line position. In (b) arrows indicate new lines of the cotunnite phase; stars indicate the reappearing fluorite phase upon shock release. Fractions refer to intensity scaling done for display purposes. “Au” in (c) marks diffraction lines of the gold pressure calibrant while “RT” stands for room temperature.

141 tunnite are visible, but the fluorite phase is compressed. 167  
 142 At 370 ns (XRD-3) the sample is at  $12.5 \pm 1$  GPa and 168  
 143 mostly in the cotunnite structure. At 523 ns  $\text{CaF}_2$  reverts 169  
 144 to a fluorite/cotunnite coexistence, as the shock 170  
 145 state releases down to between 6 and 1 GPa. The shock 171  
 146 stress necessary to induce the phase transition can be 172  
 147 bound between 7.8 GPa and 22.6 GPa.

#### 148 *XRD and Quantitative Analysis*

149 Rietveld full-profile structural refinements [26] were 175  
 150 done to confirm the phase composition in each time- 176  
 151 dependent XRD snapshot. At ambient conditions  $\text{CaF}_2$  177  
 152 starts in the fluorite structure ( $Fm\bar{3}m$ ,  $Z=4$ ), which is 178  
 153 built of a cubic close-packed array of cations, with anions 179  
 154 occupying tetrahedral sites (Fig. 4). Upon shock 180  
 155 compression to 22.6 GPa we observe the progressive de- 181  
 156 velopment of the orthorhombic cotunnite-type structure 182  
 157 ( $Pnam$ ,  $Z=4$ ). A Rietveld refinement of diffraction pat- 183  
 158 tern XRD-3 (Fig. 4) confirms that at 370 ns  $\text{CaF}_2$  fully 184  
 159 transitions to the cotunnite structure, where anions are in 185  
 160 a distorted hexagonal-close-packed lattice, while cations 186  
 161 are situated within tricapped trigonal prisms, with the 187  
 162 three outer anions in the plane of the cation [27]. We 188  
 163 estimate [20] that at 370 ns the stress state in the sample 189  
 164 is predominantly uniform at  $12.5 \pm 1$  GPa with only 10% 190  
 165 of the back of the target experiencing a gradient between 191  
 166 12 and 10 GPa.

Unit cell volumes were obtained from measured 167  
 XRD patterns (not the Hugoniot state determined via 168  
 impedance matching). Unit cell volume was evaluated, 169  
 from Rietveld full-profile structural refinements of pat- 170  
 terns labeled XRD-1 for each shot, while the sample was 171  
 in the well defined initial shock state (Fig. 4 and [20]). 172

#### 173 *Dynamic vs Static Compression*

174  $\text{CaF}_2$  was also investigated under static compression at 175  
 176 both ambient temperature and at 500K with *in-situ* XRD 177  
 178 (Fig 3(c)), under conditions designed to approximate the 179  
 180 stress and temperature states achieved in our shock ex- 181  
 182 periments. Synchrotron powder XRD in a diamond anvil 183  
 184 cell (DAC) was carried out at endstation 16-ID-B, HP- 185  
 186 CAT, of the Advanced Photon Source [20]. A comparison 187  
 188 of diffraction results under shock compression with static 189  
 189 compression reveals similarities and differences (Figs. 3 190  
 191 and 4).  $\text{CaF}_2$  undergoes the same phase transition un- 192  
 der both dynamic and static compression. A decrease in 193  
 unit cell volume at the phase transition in both types of 194  
 compression is a signature of a first-order reconstructive 195  
 transition. In Fig. 3(b) and (c) the pattern at 370 ns 196  
 (shock compression) and that at 24.1 GPa, 500K (static 197  
 compression) have the same overall shape. Shock com- 198  
 pression below or above the phase transition is character- 199  
 ized by decrease in intensity and line broadening (Fig. 3). 200  
 This is because there are two or more stress states during 201

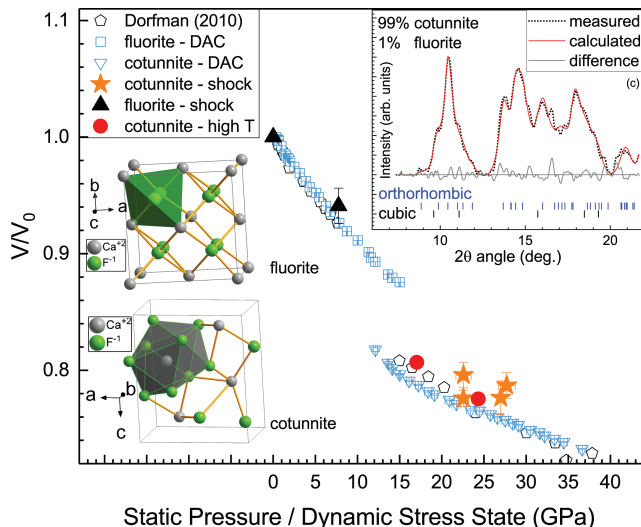


FIG. 4. The evolution of the  $\text{CaF}_2$  unit cell volume versus stress/pressure obtained from dynamic (shock) and from static compression (DAC). Solid triangles and stars represent the fluorite and cotunnite unit cell volume, respectively, under shock compression. Open squares and inverted triangles refer to static compression at 298K to 36 GPa in non-hydrostatic conditions. Solid red circles represent compression at 500K. Open pentagons are from Ref. 10. The inset on the right shows a Rietveld structural refinement at 370 ns, of the shock-driven phase transition from fluorite to cotunnite.

shock compression (decrease by factor of 2 or 3) and because the transition is from a highly symmetric structure to a lower symmetry one (factor of 3).

Dynamic compression is accompanied by shock-induced heating. For a single crystal of  $\text{CaF}_2$  we estimate the shock temperatures to be 360K at 7.7 GPa and 1000K at 33.1 GPa. Heating effects are larger in a porous sample [28]. Evidence of heating is observed (Fig. 4) in the evolution of unit cell volumes vs. stress (shock) and vs. pressure (static compression). At equivalent pressure/stress states, the shocked sample has a larger unit cell volume (between 0.5% and 2%). This departure from static (cold) compression grows with increased shock of compression, because shock-induced heating becomes more significant as the stress state increases.

### Kinetics of the Phase Transition

Plate impact, shock compression experiments provide a short, steady shock wave, without spatial stress gradients as the shock wave traverses the sample for the first time (state-1). For the experiment shown in Fig. 3(b), the initial shock transit is  $\sim 146$  ns. Thus, if the phase transition were instantaneous, only cotunnite phase would exist in the diffraction pattern at 216 ns (XRD-2). Instead, we still observe a compressed fluorite/cotunnite mixture although the pressure throughout the sample is greater than the transition threshold pressure. Not until  $\sim 370$  ns (XRD-3) where a nearly steady stress state exists, with 90% of the sample at  $12.5 \pm 1$

221 GPa (Fig. 4 and [20]), do we observe a nearly complete transition to the cotunnite structure

223 Our experiments under static compression show the co-  
224 existence of phases over a range of pressures between 11  
225 GPa and 16 GPa in  $\text{CaF}_2$  and point to a sluggish phase  
226 transition driven by diffusion, consistent with Yel'kin  
227 et. al [12]. Upon decompression, both the shock and  
228 the static compression-driven transitions show significant  
229 hysteresis. Under static compression, upon decrease of  
230 pressure from 24 GPa at 500 K the transition is found to  
231 be completely reversible, but not until 2 GPa (Fig 3(c)).  
232 Under shock compression, at 523 ns, the stress distribu-  
233 tion in the sample is between 6 and 1 GPa [20]. In the  
234 corresponding XRD pattern, we observe a reversibility  
235 to fluorite, yet with significant co-existence of the co-  
236 tunnite phase, below 7.8 GPa, which is the estimated  
237 lower bound of the phase transformation. At such a late  
238 time, edge effects are likely affecting the sample, espe-  
239 cially along the angled path of the x-ray beam.

240 Static compression and shock-driven phase transitions,  
241 especially first-order, are usually of mixed type, with  
242 essentially unexplored kinetics. The results of our *in-*  
243 *situ* XRD experiments on  $\text{CaF}_2$  and of analysis of phase  
244 percentages from Rietveld refinements allow us to ana-  
245 lyze quantitatively phase transition kinetics under shock  
246 compression by using the classical formulation of nu-  
247 cleation, developed independently by Kolmogorov [29],  
248 Johnson and Mehl [30], and Avrami [31–33] (KJMA), but  
249 applied to processes in the nanosecond timescale [20].

250 We describe the volume fraction of the cotunnite phase  
251  $\alpha(t)$  formed in the process of a shock-driven transition,  
252 during time  $t$  using the KJMA model:

$$\alpha(t) = 1 - \exp(-(k(t - \tau))^N) \quad (1)$$

253 The Avrami parameter  $N$ , is indicative of heteroge-  
254 neous or homogeneous nucleation and changes from 0.3 to  
255 4, depending on growth mechanisms.  $\tau$  is the transition  
256 incubation time and  $k$  is the crystallization rate constant.  
257 We note that the applicability of the KJMA formalism  
258 for quantification of polymorphic transitions under shock  
259 compression with an abrupt volume change must be ap-  
260 proached carefully since the formalism was developed for  
261 transformations between isotropic phases with a small  
262 volume jump and a zero shear modulus. In our anal-  
263 ysis, we group the shots to stresses between 22 and 27  
264 GPa as a first approximation that only considers stress  
265 as being sufficient to induce the phase transitions, be-  
266 cause the temperature difference between those stresses  
267 is small. While an imperfect approach, it nonetheless  
268 provides insight into the kinetics of the fluorite-cotunnite  
269 phase transition.

270 Figure 5 shows the phase concentration data and var-  
271 ious KJMA fits. The best fit to our data results in  $\tau$   
272 = 36.3 ns,  $N = 0.19$  and  $k = 2.9 \times 10^{-4}$ . This fit sug-  
273 gests a phase transition characterized by an incubation

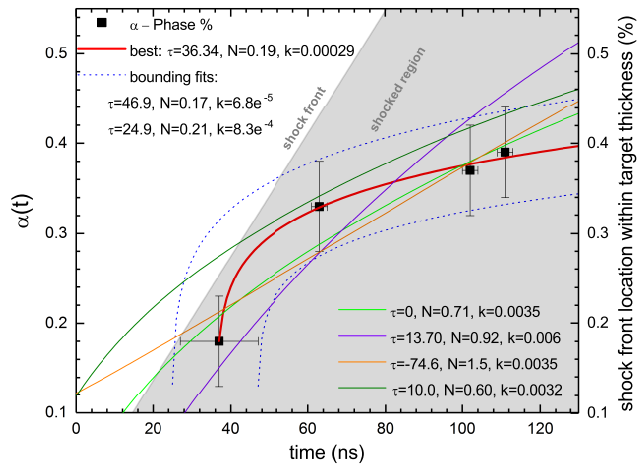


FIG. 5. Phase percentage versus time. The phase transition lags behind the shock front, marked with a grey line. The colored lines are various fits to the data using the KJMA formalism of Eqn 1.

time  $\tau \sim 36 \pm 1$  ns [20]. This is consistent with the transition delay hinted at in a visual inspection of our time-dependent XRD patterns (Fig. 3). The incubation time, along with the hysteresis on stress release, suggests a first-order reconstructive transition and points to a kinetic barrier that impedes the transition at the equilibrium pressure of the two phases. The incubation time is comparable with shock compression of various materials, from 6 ns to 10's of ns [4, 34]. Figure 5 shows that the phase transformation rate is initially fast, but slows when the cotunnite phase percentage reaches  $\sim 30\%$ . Under static compression, Yelkin *et al* [12] observed a similar slowdown in the transition rate around  $\alpha \sim 20\%$ - $30\%$ .

Our fitted  $N = 0.19 \pm 0.04$  [20] indicates an inhomogeneous distribution of nucleation sites [35] and points to a distribution of grain sizes, where transformation begins on the surface of grains. It was found that heterogeneous nucleation and likely simultaneous diffusion-controlled crystallization correspond to  $N \leq 1$  [36]. Our Avrami parameter is also consistent with  $N \sim 0.1$  found under static compression [12] for the stage when more than  $\sim 20\%$ - $30\%$  cotunnite is formed. Forcing  $N > 1$  produces negative incubation times (see [20]). Using molecular dynamics simulations, Boulfefel [37] showed that the pressure-induced transition in  $\text{CaF}_2$  is characterized by nucleation and growth of the new phase, with local melting of the fluoride sublattice, which produces defects, followed by recrystallization into the cotunnite structure. Our results are consistent both with local melting (long incubation time) and with heterogeneous nucleation and growth processes (low Avrami parameter).

We demonstrated a shock-driven phase transition in an ionic solid, on nanosecond time scales and at a microstructural level from a more ordered to a less ordered structure. Time-resolved XRD illustrates the un-

folding of the reconstructive phase transition and hysteresis on unloading. A direct comparison of unit cell volumes between dynamic and static loading points to measurable structural effects of temperature on increased shock loading. The ability to combine *in situ* XRD measurements with well-characterized shock loading experiments now allows for Rietveld, full-profile structural refinements that lead to analysis of the phase concentrations. Our results give insight into the kinetic timescale of the fluorite-cotunnite phase transition under shock compression, which is relevant to a number of isomorphous compounds. These methods and results can be used to develop improved kinetic models for complex, solid-solid phase transitions.

**The authors are grateful** to Dr. Thomas Mattsson, SNL, for a critical reading of the manuscript and valuable advice. We also thank the two anonymous reviewers whose comments greatly improved the paper. The authors thank the people at that contributed to the design, fabrication, and fielding of the experiments at SNL, at DCS-APS and at HPCAT-APS. Sandia National Laboratories is a multimission laboratory managed and operated by National Technology and Engineering Solutions of Sandia, LLC., a wholly owned subsidiary of Honeywell International, Inc., for the U.S. Department of Energy's National Nuclear Security Administration under contract DE-NA-0003525. Portions of this work performed at the Dynamic Compression Sector supported by the Department of Energy, National Nuclear Security Administration, under Award Number DE-NA0002442 and operated by Washington State University. Portions of this work were performed at HPCAT (Sector 16), Advanced Photon Source (APS), Argonne National Laboratory. HPCAT operations are supported by DOE-NSA under Award No. DE-NA0001974, with partial instrumentation funding by NSF. J.S. and S.S. acknowledge the support of DOE-BES/DMSE under Award DE-FG02-99ER45775 The Advanced Photon Source is a U.S. Department of Energy (DOE) Office of Science User Facility operated for the DOE Office of Science by Argonne National Laboratory under Contract No. DE-AC02-06CH11357. Work at HiPSEC is supported by the National Nuclear Security Administration under the Stewardship Science Academic Alliances program through DOE Cooperative Agreement DE-NA0001982.

\* pekalic@sandia.gov

- [1] D. Milathianaki, S. Boutet, G. J. Williams, A. Higginbotham, D. Ratner, A. E. Gleason, M. Messerschmidt, M. M. Seibert, D. C. Swift, P. Hering, J. Robinson, W. E. White, and J. S. Wark, *Science* **342**, 220 (2013).
- [2] A. Higginbotham, P. G. Stubley, A. J. Comley, J. H. Eggert, J. M. Foster, D. H. Kalantar, D. McGonegle, S. Patel, L. J. Peacock, S. D. Rothman, R. F. Smith,

- 362 M. J. Suggit, and J. S. Wark, *Sci Rep-UK* **6** (2016).  
 363 [3] S. J. Turneaure, N. Sinclair, and Y. M. Gupta, *Phys.*  
 364 *Rev. Lett.* **117**, 045502 (2016).  
 365 [4] A. . Gleason, C. . Bolme, E. Galtier, H. . Lee, E. Grana-  
 366 dos, D. . Dolan, C. . Seagle, T. Ao, S. Ali, A. Lazicki,  
 367 D. Swift, P. Celliers, and W. . Mao, *Phys. Rev. Let.* **119**,  
 368 025701 (2017).  
 369 [5] K. F. Seifert, *Berich. Bunsen. Gesell.* **70**, 1041 (1966).  
 370 [6] D. Dandekar and J. Jamieson, *Trans. Am. Cryst.* **5**, 19  
 371 (1969).  
 372 [7] L. Gerward, J. S. Olsen, S. Steenstrup, M. Malinowski,  
 373 S. Asbrink, and A. Waskowska, *J. Appl. Crystallogr.* **25**,  
 374 578 (1992).  
 375 [8] X. Wu, S. Qin, and Z. Wu, *Phys. Rev. B* **73**, 134103  
 376 (2006).  
 377 [9] H. Shi, W. Luo, B. Johansson, and R. Ahujia, *J. Phys-*  
 378 *Condensed Matter* **21**, 415501 (2009).  
 379 [10] S. M. Dorfman, F. Jiang, Z. Mao, A. Kubo, Y. Meng,  
 380 V. B. Prakapenka, and T. S. Duffy, *Phys. Rev. B* **81**,  
 381 174121 (2010).  
 382 [11] J. R. Nelson, R. J. Needs, and C. J. Pickard, *Phys. Rev.*  
 383 *B* **95**, 054118 (2017).  
 384 [12] F. S. Yelkin, O. B. Tsiok, V. V. Brazhkin, and L. G.  
 385 Khvostantsev, *Phys. Rev. B* **73**, 094113 (2006).  
 386 [13] A. Kavner, *Phys. Rev. B* **77**, 224102 (2008).  
 387 [14] G. A. Adadurov, Z. G. Aliyev, L. O. Atovmyan, Y. G.  
 388 Borod'ko, O. N. Breusov, A. N. Dremin, A. K. Mu-  
 389 ranevich, and N. P. Khrameyeva, *Bull. (Izv), Acad. Sci.*  
 390 *USSR, Inorg. Materials* **3**, 6 (1965).  
 391 [15] V. N. German, N. N. Orlova, M. N. Pavlovskii, L. A.  
 392 Tarasova, and R. F. Trunin, *Izv. AN. Nauk SSSR Fiz.*  
 393 *Zemli* **8**, 12 (1975).  
 394 [16] M. Hasegawa, K. Kondo, and A. Sawaoka, *Jpn J Appl.*  
 395 *Phys.* **23**, 20 (1984).  
 396 [17] T. Sekine and T. Kobayashi, *Phys Chem Miner* **38**, 305  
 397 (2011).  
 398 [18] W. Carter and S. Marsh, *Hugoniot Equation of State of*  
 399 *Polymers LA-13006-MS*, Report (Los Alamos National  
 400 Laboratory, 1995).  
 401 [19] S. Root, T. R. Mattsson, K. Cochrane, R. W. Lemke,  
 402 and M. D. Knudson, *J. Appl. Phys.* **118** (2015).  
 403 [20] "See supplemental materials at  
 404 <http://link.aps.org/supplemental/>, which include  
 405 additional experimental details and results for dy-  
 406 namic and static compression experiments, methods  
 407 for estimating stress distribution in targets, and results  
 408 of rietveld structural refinements and includes the  
 409 references [18, 23, 25, 38–45]".  
 410 [21] L. V. Al'tshuler, M. A. Podurets, G. V. Simakov, and  
 411 R. F. Trunin, *Sov. Phys. Solid State* **15**, 969 (1973).  
 412 [22] T. Taniguchi, K. Kondo, and A. Sawaoka, *J. Appl. Phys.*  
 413 **61**, 196 (1987).  
 414 [23] O. T. Strand, D. R. Goosman, C. Martinez, T. L. Whit-  
 415 worth, and W. W. Kuhlow, *Rev. Sci. Instrum.* **77**,  
 416 083108 (2006).  
 417 [24] G. E. Duvall and R. A. Graham, *Rev. Mod. Phys.* **49**,  
 418 523 (1977).  
 419 [25] S. Root, L. Shulenburg, R. W. Lemke, D. H. Dolan,  
 420 T. R. Mattsson, and M. P. Desjarlais, *Phys. Rev. Lett.*  
 421 **115**, 198501 (2015).  
 422 [26] H. M. Rietveld, *J. Appl. Crystallogr.* **2**, 65 (1969).  
 423 [27] E. Morris, T. Groy, and K. Leinenweber, *J. Phys. Chem.*  
 424 *Solids* **62**, 1117 (2001).  
 425 [28] G. Fenton, D. Grady, and T. Vogler, *J. Dynamic Behav-*  
 426 *ior Mater.* **1**, 103 (2015).  
 427 [29] A. Kolmogorov, *Bull. Acad. Sci. USSR Phys. Ser.* **3**, 555  
 428 (1937).  
 429 [30] W. Johnson and R. Mehl, *Trans. Am Inst. Min. Eng.*  
 430 **135**, 416 (1939).  
 431 [31] M. Avrami, *J. Chem. Phys.* **7**, 1103 (1939).  
 432 [32] M. Avrami, *J. Chem. Phys.* **8**, 212 (1940).  
 433 [33] M. Avrami, *J. Chem. Phys.* **9**, 177 (1941).  
 434 [34] K. Ichiyanagi and K. G. Nakamura, *Metals* **6** (2016).  
 435 [35] N. X. Sun, X. D. Liu, and K. Lu, *Scripta Materialia* **34**,  
 436 1201 (1996).  
 437 [36] J. A. Lopes-Da-Silva and J. A. P. Coutinho, *Energy &*  
 438 *Fuels* **21**, 3612 (2007).  
 439 [37] S. E. Boulfelfel, D. Zahn, O. Hochrein, Y. Grin, and  
 440 S. Leoni, *Phys. Rev. B* **74**, 094106 (2006).  
 441 [38] T. Ao and D. H. Dolan, *SIRHEN: a data reduction pro-*  
 442 *gram for photonic Doppler velocimetry measurements -*  
 443 *SAND2010-3628*, Report (Sandia National Laboratories,  
 444 2010).  
 445 [39] C. Prescher and V. B. Prakapenka, *High Pressure Res.*  
 446 **35**, 223 (2015).  
 447 [40] O. L. Anderson, D. G. Isaak, and S. Yamamoto, *J. Appl.*  
 448 *Phys.* **65**, 1534 (1989).  
 449 [41] J. M. McGlaun, S. L. Thompson, and M. G. Elrick, *Int.*  
 450 *J. Impact Eng.* **10**, 351 (1990).  
 451 [42] W. Herrmann, *J. Appl. Phys.* **40**, 2490 (1969).  
 452 [43] M. Carroll and A. C. Holt, *J. Appl. Phys.* **43**, 759 (1972).  
 453 [44] G. R. Johnson and W. H. Cook, in *Proceedings of the*  
 454 *7th International Symposium on Ballistics* (The Hague,  
 455 Netherlands, 1983) p. 541.  
 456 [45] G. R. Johnson and W. H. Cook, *Eng. Fract. Mech.* **21**,  
 457 31 (1985).